npj | clean water

www.nature.com/npjcleanwater

ARTICLE OPEN

Check for updates

# Selective removal of $Na^+$ by $NaTi_2(PO_4)_3$-MWCNT composite hollow-fiber membrane electrode in capacitive deionization

Joosung Park[1], Mi-Young Lee[1], Seungyeob Han[1], Keun-Young Lee[2] and Seoktae Kang[1]✉

In this study, $NaTi_2(PO_4)_3$ (NTP) nanoparticles were incorporated into a carbon nanotube hollow-fiber (CHF) electrode for the selective removal of $Na^+$ during the capacitive deionization (CDI) of salty water. Due to the $Na^+$-selective electro-sorption of NTP nanoparticles, NTP-CHF achieved 1.5 ~2 times higher $Na^+$ adsorption capacity than that of CHF only electrodes at a range of 1.7 mM~17.1 mM (100 mg $L^{-1}$~1000 mg $L^{-1}$) NaCl solution. Moreover NTP-CHF sustained the $Na^+$ adsorption capacity even at the presence of $Ca^{2+}$ ions, whereas the dramatic decrease in $Na^+$ removal was observed in CHF with an increase of $Ca^{2+}$ concentration. As the result, NTP-CHF can retain 52% of the initial $Na^+$ removal capacity after three times of capture and release cycles at the presence of $Ca^{2+}$, while CHF showed <10% of the initial $Na^+$ removal capacity due to the irreversible adsorption of $Ca^{2+}$ ions onto the MWCNT surface. Thus, the incorporation of NTP into the conductive carbon nanomaterial network can greatly improve both the adsorption capacity and selectivity of $Na^+$ compared to the conventional carbon-based electrode during the CDI of salty water containing multivalent cations such as $Ca^{2+}$.

*npj Clean Water* (2022)5:14; https://doi.org/10.1038/s41545-022-00156-3

## INTRODUCTION

Capacitive deionization (CDI) is an emerging desalination technology that adsorbs ions in water by a porous electrode based on an electric double layer capacitor (EDLC). Compared with commercialized desalination technologies such as reverse osmosis (RO) and thermal processes, CDI is known to have advantages in terms of energy consumption and maintenance for low salt water[1,2].

During the operation of CDI, the ion removal performance is highly dependent on the properties of the electrodes such as the specific surface area, effective pore size, electric conductivity, water wettability, and ion accessibility[1,3–5]. In practice, CDI electrodes are generally produced in a metal plate form by coating various electrode materials on the surface of non-permeable metal plates. Among various electrode materials, carbon allotropes including activated carbons[6–9], carbon fibers and aerogels[10,11], carbon nanotubes[12,13], and graphene[14,15], have been most frequently used as CDI electrodes incorporating with metal (oxide) nanoparticles[15–18] (Table S1). However, there are several challenges for the application of carbon materials as CDI electrodes that the ion transport strongly depends on the electric field-assisted diffusion, which induces a slow adsorption rate of ions onto the electrode[19]. The electrical double layer (EDL) overlapping or a co-ion repulsion effect also hinders the removal of ions[20,21]. In addition, irreversible adsorption of multivalent ions such as $Ca^{2+}$, $Mg^{2+}$, or $SO_4^{2-}$ also lead to a significant decrease in the ion removal capacity, especially during repeated uses[22,23]. These issues are mainly caused by the ion removal mechanism of the carbon nanomaterial-based electrodes: target ions adsorbed on the surface of the electrode by non-Faradaic reaction without any charge neutralization.

To resolve the above issues, both physical and chemical approaches have been explored. As an example, we reported a CNT-based hollow fiber electrode (CHF) to improve the physical characteristics of the electrode[24]. In this electrode, the salty water can flow through the electrode, thus, the ion transfer is mainly occurred much faster by convection, while that of a conventional plate-type electrode is slower by diffusion. As a result, the CHF electrode achieved faster ion removal kinetics (i.e., <10 min to reach maximum ion adsorption and desorption capacity) and higher ion removal capacity (58.2 mg $g^{-1}$ at 500 mg $L^{-1}$ NaCl solution). Despite the improvement in the study, the CHF did not solve the problem of non-selective and irreversible ion adsorption at the presence of multivalent ions such as $Ca^{2+}$.

To overcome the irreversible adsorption of multivalent ions onto carbon-based CDI electrodes, various methods have been applied including the incorporation of nanoparticles and membrane-assisted CDI (MCDI). Metal nanoparticles such as $MnO_2$, $Fe_3O_4$, $Co_3O_4$, Mn-polypyrrole composite[4] and a metal-organic framework[18] have been applied to form the composite structure with carbon materials and exhibited enhanced removal of ions[3,4,15,17,18]. However, the ion removal mechanism of these electrodes were highly dependent on a non-Faradaic reaction[25], therefore, multivalent ions were still preferably adsorbed on the surface of a CDI electrode compared to monovalent ions such as $Na^+$, as well as exhibited more irreversible desorption. For a stable and reversible CDI process under the presence of multivalent cations, the MCDI with ion exchange membranes[26] or ion exchange resin coatings[27] has been developed. In these electrodes, multivalent ions can be desorbed by applying a reverse potential to the electrodes, thus, the CDI performance can be sustained under the presence of multivalent ions such as $Mg^{2+}$ or $Ca^{2+}$. However, the performance of MCDI is significantly varied by the performance and configurations of ion exchange membranes. Moreover, MCDI cannot solve the EDL overlapping phenomenon,

[1]Department of Civil and Environmental Engineering, Korea Advanced Institute of Science and Technology, 291 Daehak-ro, Yuseong-gu, Daejeon 34141, Republic of Korea. [2]Decommissioning Technology Research Division, Korea Atomic Energy Research Institute, 111 Daedeok-daero 989 Beon-gil, Yuseong-Gu, Daejeon 34057, Republic of Korea. ✉email: stkang@kaist.ac.kr

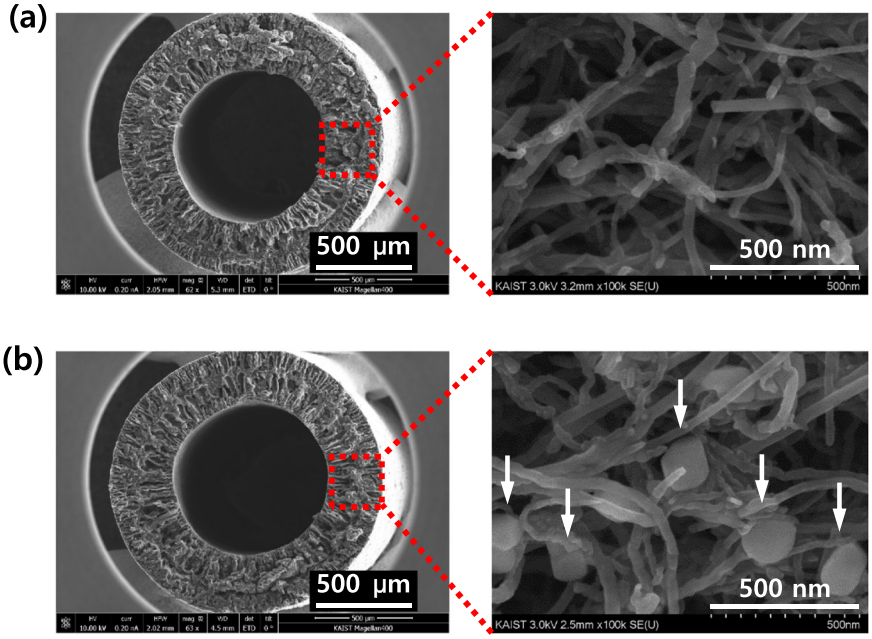


**Fig. 1 SEM images at various magnifications. a** CHF and **b** NTP-CHF.

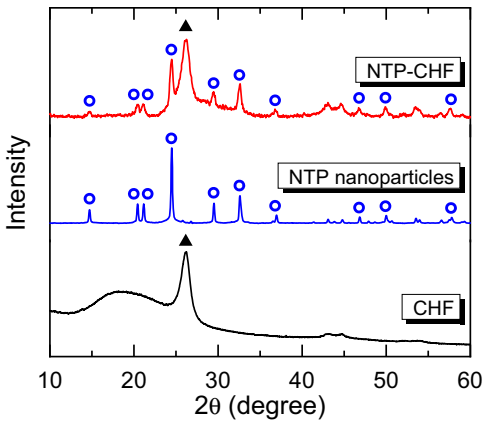


**Fig. 2** XRD patterns of CHF, NTP nanoparticles, and NTP-CHF.

which reduces ion removal capacity of carbon-based, non-Faradaic ion removal electrodes.

To solve both issues in CDI electrodes, the incorporation of Faradaic reaction-based $Na^+$-selective materials to the cathode materials can be the potential solution. When $Na^+$-selective materials are incorporated on the cathode, the removal of multivalent ions will be effectively hindered based on the selectivity of the $Na^+$-capturing materials. Among various candidate materials, $NaTi_2(PO_4)_3$ (NTP) has been reported to possess the high ionic conductivity, reversible capacity, and chemical characteristics[28–31]. In addition, NTP affords not only reversible capture and release of $Na^+$ ion into its crystal structure by Faradaic reaction, but also provides the selective removal of $Na^+$ in the presence of multivalent cations such as $Ca^{2+}$ and $Mg^{2+}$[32]. According to the theoretical calculations, the maximum $Na^+$ removal capacity of NTP is 4.78 mmol $g^{-1}$, which is much higher than that of metal oxide-carbon composite-based CDI electrodes[33].

On the basis of this rationale, NTP nanoparticles were synthesized and then incorporated into CHF structures (NTP-CHF) to provide both convective transport of ions into cationic adsorbents and Faradaic selective removal of $Na^+$-. Moreover, the cation adsorption capacity and reversibility of NTP-CHF were evaluated at the presence of $Ca^{2+}$ as a model multivalent cation to verify selective $Na^+$ removal characteristics of NTP-CHF in the CDI process.

**Table 1.** Physical properties of CHF and NTP-CHF.

| | Surface area [$m^2$ $g^{-1}$] | Pore volume [$cm^3$ $g^{-1}$] | Pore size [nm] |
|---|---|---|---|
| CHF | 77.81 | 0.219 | 43.95 |
| NTP-CHF | 60.28 | 0.199 | 24.01 |

## RESULTS AND DISCUSSION

### Physicochemical properties of CHF and NTP-CHF

SEM images of CHF and NTP-CHF are shown in Fig. 1. Both electrodes have a uniform hollow-fiber structure with the outer and inner diameters around 1.4 mm and 0.8 mm, respectively. The SEM image of NTP-CHF showed that NTP nanoparticles were successfully combined and formed an effective electric network in the entangled MWCNT structure (Fig. 1b). The EDX mapping of the surface of NTP-CHF also exhibited that titanium and phosphorous, major organizing elements of NTP, were detected on the whole region of NTP-CHF (Supplementary Fig. 2). XRD analysis of CHF, pristine NTP nanoparticles, and NTP-CHF were carried out, and the results are presented in Fig. 2. It showed that the XRD pattern of NTP-CHF clearly matched with that of CHF (PDF no. 01-075-1621) and bare NTP nanoparticles (PDF no. 00-033-1296). In addition, there was no noticeable peak shift or new peak from NTP-CHF compared to CHF or the NTP nanoparticles, which indicated that the NTP and MWCNTs in the NTP-CHF structure did not experience any chemical structural changes. In summary, NTP nanoparticles were successfully anchored and incorporated in the structure of MWCNT networks in NTP-CHF.

The specific surface area and the pore characteristics summarized in Table 1 showed that NTP-CHF exhibited a decreased specific surface area compared to that of CHF due to the higher density of NTP nanoparticles than MWCNTs in NTP-CHF.

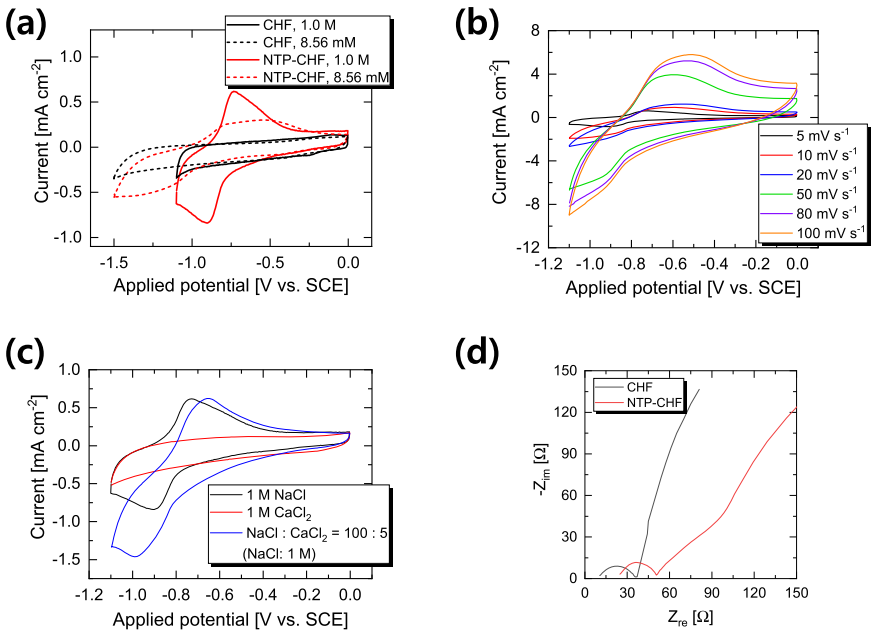


**Fig. 3 Electrochemical properties of CHF and NTP-CHF.** Cyclic voltammetry curves (**a**) in 1 M and 8.6 mM NaCl solutions at 5 mV $s^{-1}$, (**b**) under various scanning rates, and **c** in the presence and absence of $Ca^{2+}$, (**d**) Nyquist plots of CHF and NTP-CHF. Note that NTP-CHF was used as electrodes in (**b**) and (**c**), and all tests were performed in 1 M NaCl solution otherwise noted.

**Table 2.** Electrochemical properties of CHF and NTP-CHF in NaCl solutions.

| NaCl concentration | CHF | | NTP-CHF | |
|---|---|---|---|---|
| | Specific capacitance [F $g^{-1}$] | Specific capacity [C $g^{-1}$] | Specific capacitance [F $g^{-1}$] | Specific capacity [C $g^{-1}$] |
| 1 M (58.4 g $L^{-1}$) | 5.7 | 6.3 | 14.9 | 16.4 |
| 8.6 mM (500 mg $L^{-1}$) | 5.3 | 7.9 | 9.5 | 14.2 |
| 1.7 mM (100 mg $L^{-1}$) | 3.4 | 6.8 | 5.9 | 11.8 |

Both electrodes have a mesoporous pore structure, which enables faster ion transport through pores.

### Electrochemical characteristics of CHF and NTP-CHF

Figure 3a displays the CV curves of CHF and NTP-CHF in various concentrations of NaCl. In this analysis, CHF presents the typical capacitive behaviour of a non-Faradaic reaction-based electric double layer capacitor (EDLC). However, NTP-CHF showed not only a non-Faradaic reaction but also a reduction peak at −0.9 V and an oxidation peak at −0.7 V in 1.0 M NaCl solution. The reduction and oxidation peaks indicate that NTP-CHF is successfully adsorbing and desorbing $Na^+$ ions by a Faradaic reaction of NTP nanoparticles in addition to non-Faradaic reaction of MWCNTs[28], while CHF adsorbs $Na^+$ by only a non-Faradaic reaction. At 8.6 mM NaCl solution, the reduction peak was shifted to −1.2 V due to the decrease in ionic conductivity of the feed solution. The calculated specific capacity at the standard condition (i.e., 1 M NaCl) exhibited that NTP-CHF was significantly higher (16.4 C $g^{-1}$) than that of CHF (6.3 C $g^{-1}$) as shown in Table 2. At various NaCl concentrations, NTP-CHF always showed about two times higher specific capacity than CHF, and as discussed above, it is mainly originated from NTP nanoparticles in NTP-CHF. During the increase of scanning rate of cyclic voltammetry from 5 mV $s^{-1}$ to 100 mV $s^{-1}$ with NTP-CHF (Fig. 3b), overpotential for $Na^+$ absorption-desorption reaction gradually magnified and specific capacity decreased from 16.4 C $g^{-1}$ to 4.3 C $g^{-1}$ (Supplementarty Table 2) due to the slower kinetics of Faradaic reaction of NTP nanoparticles than non-Faradaic reaction by CHF.

The Na-selective adsorption of NTP-CHF in the mixture of $Na^+$ and $Ca^{2+}$ was evaluated by cyclic voltammetry (Fig. 3c). In 1 M $CaCl_2$ solution, NTP-CHF did not show Faradaic reaction because NTP did not absorb $Ca^{2+}$ from electrolyte. In case of 1 M NaCl or the mixture with $CaCl_2$ (NaCl: $CaCl_2$ = 100: 5), NTP-CHF successfully absorb and desorb $Na^+$ ions from electrolyte with increased difference between anodic peak potential and cathodic peak potential from 172 mV to 335 mV. It is mainly caused by the selective adsorption of $Na^+$ by NTP nanoparticles incorporated in NTP-CHF.

The electrochemical impedance spectroscopy (EIS) analysis showed that both hollow-fiber electrodes have one semi-circle at high frequency and linear region at low frequency in the Nyquist plot (Fig. 3d). Both electrodes showed similar semi-circle region with the electrode resistance of 10.7 Ω and 24.8 Ω for CHF and NTP-CHF, respectively. In the low frequency (or higher impedance) region, NTP-CHF showed lower slope than that of CHF, which implied that NTP-CHF had Faradaic capacitive regime, while CHF had a diffusion controlled adsorption regime[34,35].

### Capture and release characteristics of $Na^+$ by CHF and NTP-CHF

Results from Fig. 3 and Table 2 strongly implied that NTP-CHF has a higher ion adsorption capacity than CHF. Thus, the $Na^+$ removal capacity of both electrodes under 1.3 V were examined at 1.7, 4.3, 8.6, and 17.1 mM NaCl solutions. As shown in Fig. 4, NTP-CHF always exhibited higher $Na^+$ adsorption capacity not only than CHF, but also than other carbon-based electrodes (Supplementary Table 1).

It is due to the highly developed pores in a hollow-fiber structure as previously reported[24], and the Faradaic ion adsorption characteristics of the NTP nanoparticles in NTP-CHF. More specifically, as shown in the CV analysis in Fig. 3, CHF adsorbs $Na^+$ ions by the non-Faradaic reaction, while NTP-CHF could adsorb $Na^+$ by both the non-Faradaic reaction of MWNCTs and the reversible Faradaic reaction by NTP nanoparticles.

In general, the Faradaic reaction such as $Na^+$ adsorption by NTP nanoparticles exhibits slower reaction kinetics than the non-Faradaic reaction. To evaluate the adsorption kinetics of NTP-CHF and CHF, $Na^+$ adsorption capacities of NTP-CHF and CHF were tested under the 8.6 mM NaCl solution at the 1.3 V of applied potential. As shown Fig. 5a, both CHF and NTP-CHF reached their maximum adsorption capacity within 15 min, and NTP-CHF showed 1.5 times higher (2.2 mmol $g^{-1}$) adsorption capacity than that of CHF. The Ragone curve of NTP-CHF located at the upper-right side of CHF (Fig. 5b), thus NTP-CHF had higher $Na^+$ adsorption rate and capacity than those of CHF at the same condition[36]. It is due to the highly porous network of MWCNTs which provides sufficient electrons for the Faradaic $Na^+$ adsorption reaction of incorporated NTP nanoparticles, and results in fast reaction kinetics comparable with the MWCNT-only electrode (CHF).

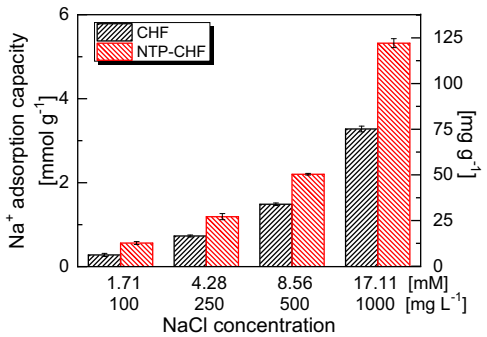


**Fig. 4 Na+ adsorption capacity of CHF and NTP-CHF at various NaCl concentrations.** Error bars represent standard deviations.

The electrochemical characteristics of hollow-fiber electrodes were also evaluated by galvanostatic charge-discharge test (Fig. 5c). In this experiment, NTP-CHF shows the pair of Faradaic charge and discharge reaction by NTP nanoparticles, which is not observed in CHF. Thus, Faradaic adsorption of $Na^+$ by NTP nanoparticles is responsible for the increased adsorption capacity of NTP-CHF.

The cyclic adsorption-desorption curves in Fig. 5d exhibited that NTP-CHF could be operated without a significant loss of the $Na^+$ adsorption capacity during 50 times of adsorption-desorption cycles at 1.3 V in 8.6 mM NaCl solution. It has been reported that bare NTP nanoparticles have highly irreversible capacity in the initial charging and discharging process due to their low electric conductivity[28]. However, NTP nanoparticles in NTP-CHF were incorporated in the porous structure of highly conductive MWNCTs, thus, MWCNT structures provided the better ion transport as well as the faster electron transfer. After 50 cycles of ion adsorption-desorption, $Na^+$ adsorption capacity of CHF decreased to 52% of initial value (0.76 mmol $g^{-1}$), while NTP-CHF kept 68% of its initial performance (1.51 mmol $g^{-1}$). These results can be found in many other studies and explained that the reduction of adsorption capacity after the repeated cyclic operation mainly came from the changes in electrochemical surface properties of MWCNTs in CHF and NTP-CHF, where NTP nanoparticles in NTP-CHF kept original properties more than CHF[28,37,38]. In addition to the electrochemical surface modification, irreversible adsorption of $Ca^{2+}$ also plays an important role for the decrease in $Na^+$ removal efficiencies in long-term operation of CDI in the next section.

### Impact of $Ca^{2+}$ ions to $Na^+$ removal efficiencies

For the carbon-based CDI electrode, multivalent cations such as $Ca^{2+}$ bound irreversibly and led to low regeneration efficiency during the repeated use of CDI electrodes[22]. To evaluate the

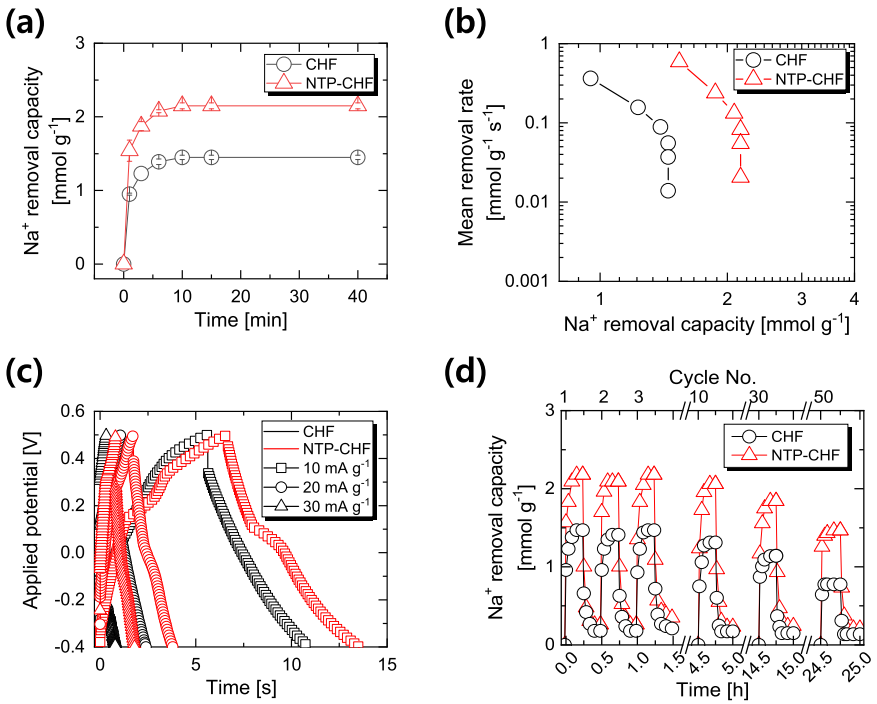


**Fig. 5 Na+ adsorption/desorption characteristics of hollow-fiber electrodes under 8.6 mM NaCl solution. a** Adsorption kinetics, (**b**) Ragone plot, (**c**) Galvanostatic curves for NTP-CHF at various current densities, and (**d**) Cyclic adsorption-desorption curve.

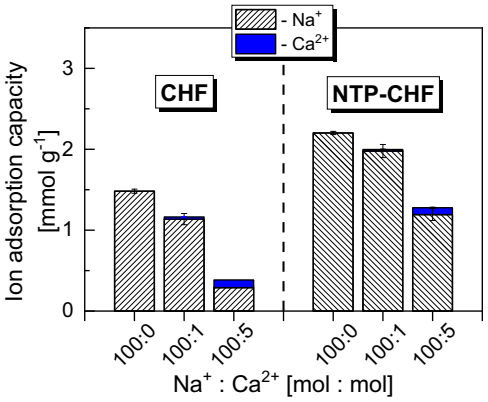


**Fig. 6 Changes in ion adsorption capacity at various $Na^+$:$Ca^{2+}$ ratio.** Note that the $Na^+$ concentration and the applied electric potential were fixed at 8.6 mM and 1.3 V, respectively. Error bars represent standard deviations.

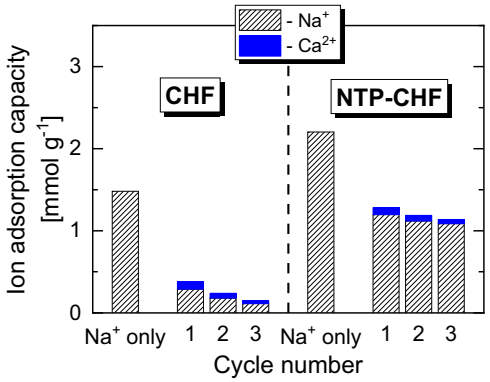


**Fig. 7** Changes in cation adsorption capacities during repeated adsorption and desorption cycles in the presence of 0.43 mM of $Ca^{2+}$ in 8.6 mM of $Na^+$ ($Na^+$:$Ca^{2+}$ = 100:5).

impact of $Ca^{2+}$ ions during the removal of $Na^+$, the molar ratio of $Na^+$:$Ca^{2+}$ was adjusted from 100:0 to 100:5, and the ion removal capacities were measured.

As expected, the impact of $Ca^{2+}$ ions became more pronounced with an increase of $Ca^{2+}$ concentration as shown in Fig. 6. The $Na^+$ removal capacity of CHF dramatically decreased from 1.48 mmol $g^{-1}$ to 0.29 mmol $g^{-1}$ when 0.43 mM of $Ca^{2+}$ was added into the feed solution ($Na^+$:$Ca^{2+}$ = 100:5). However, at the same condition, the $Na^+$ removal capacity of NTP-CHF decreased from 2.20 mmol $g^{-1}$ to 1.19 mmol $g^{-1}$. The decrease in $Na^+$ removal capacities of CHF and NTP-CHF was due to the occupation of ion capturing sites by more strongly bound $Ca^{2+}$ ions as well as by the larger hydration radius of $Ca^{2+}$ than $Na^+$, which hindered the access of $Na^+$ ions to the capturing sites[22,39].

Importantly, it should be noted that the impact of $Ca^{2+}$ ions was only limited to the capturing sites on MWCNTs. As shown in Fig. 6, the decreased amount of $Na^+$ removal capacities of CHF were 0.34 mmol $g^{-1}$ and 1.19 mmol $g^{-1}$ at 100:1 and 100:5 of $Na^+$:$Ca^{2+}$ ratios, respectively, and the values are almost identical with those of NTP-CHF (0.22 mmol $g^{-1}$ and 1.01 mmol $g^{-1}$) even at various ratios of $Na^+$:$Ca^{2+}$. It strongly implied that the impact of $Ca^{2+}$ ions was limited to the ion capturing sites on MWCNTs in CHF and NTP-CHF. This will be discussed further in the following section.

### Impact of $Ca^{2+}$ during the repeated capture-release cycles

To evaluate the cyclic impact of $Ca^{2+}$ on the removal of $Na^+$ in the CHF and NTP-CHF electrodes, the capture (15 min at 1.3 V) and release (15 min at 0 V) were repeated three times in the presence of 0.43 mM $CaCl_2$. As shown in Fig. 7, the total ion removal capacity of NTP-CHF was decreased continuously, retained 52% of the initial $Na^+$ removal capacity after three iterations of capture and release cycles, while that of CHF was only 10%. As discussed above, CHF quickly lost its $Na^+$ removal capacity by the irreversible attachment of $Ca^{2+}$ ions on MWCNTs during the repeated uses, while NTP-CHF could retain the $Na^+$ removal capacity from NTP nanoparticles under the existence of multivalent cations. In Fig. 7, the decreased amount of ion removal capacities during the capture-release cycles in the presence of $Ca^{2+}$ was identical in CHF and NTP-CHF electrodes as observed in Fig. 6. The decrements of the $Na^+$ removal capacity in each cycle were 1.19, 1.30, and 1.37 mmol $g^{-1}$ for CHF, and 1.00, 1.08, and 1.12 mmol $g^{-1}$ for NTP-CHF, respectively. This implies that $Ca^{2+}$ ions were mainly adsorbed onto MWCNT structures, and did not inhibit the electrochemical $Na^+$ ion removal by NTP nanoparticles in NTP-CHF. The selectivity of NTP nanoparticles are firstly arose from the difference in the behaviour of alkali metal and alkali earth metal in NTP. First, in the Na super ionic conductor (NASICON) type crystal structure ($NaM_2(PO_4)_3$), $Ca^{2+}$ exists at the $MO_6$ octahedral site, not at the interstitial site for $Na^+$ [40]. As a result, $Ca^{2+}$ does not impede the $Na^+$ capture-release reaction. Secondly, the ionic conductivity of multivalent ions in the NASICON crystal under room temperature is too low to transfer multivalent ions from the surface to the inner side of the crystal[41]. As result, it is clear that $Ca^{2+}$ significantly less affects the performance of NTP-CHF as a negative electrode of CDI than CHF due to the selective $Na^+$ removal reaction of NTP nanoparticles. Based on the overall results, NTP-CHF can be applied to an ion removal system where the selective removal of $Na^+$ from water is required such as in drinking water production from deep seawater.

### Concluding remarks

In this work, NTP-CHF, a $NaTi_2(PO_4)_3$-incorporated MWCNT hollow-fiber electrode, was fabricated and evaluated for $Na^+$-selective removal electrode in the CDI process. The prepared NTP-CHF has a mesoporous and water-permeable structure, which enhances the ion migration into the electrode. The incorporation of $NaTi_2(PO_4)_3$ provides synergistic effects where the MWCNTs serves as an highly conductive network for the NTP nanoparticles and NTP nanoparticles provide selective $Na^+$ removal with preventing the irreversible adsorption of multivalent cations. The novel selective removal of NTP-CHF is due to the unique crystal structure and electrochemical characteristics of NTP, and thus, shows both higher $Na^+$ removal capacity and regeneration efficiency than CHF at the presence of $Ca^{2+}$. Overall, this study proved that the incorporation of Faradaic reaction-based electrode materials such as NTP could significantly enhance ion adsorption capacities in the CDI process treating low salt solution, and moreover, the ion removal capacity was not influenced by the presence of multivalent ions such as $Ca^{2+}$ unlike conventional carbon-based CDI electrodes.

## METHODS

### Preparation of MWCNTs and NTP nanoparticles

Functionalized multi-walled carbon nanotubes (MWCNTs, diameter: 50~80 nm, length: 10~20 μm) were purchased from Cheap Tubes (USA), and further purified using 10 M HCl solution for 18 h. NTP nanoparticles were synthesized by the solvothermal method[28]. Briefly, equal molar amounts of titanium(IV) butoxide and sodium acetate were dissolved into anhydrous ethanol. The solution was then slowly mixed with a phosphorous acid solution (85 wt%) to a volumetric ratio of 1:3. After complete mixing, the solution was transferred into an autoclave and reacted at 160 °C for 3 h. After the reaction, white precipitates were separated by centrifugation and washed with deionized water. Finally, NTP

nanoparticles were obtained by drying the white precipitate with a freeze dryer (Labconco, FreeZone 6 Plus) and annealing at 600 °C in an Ar environment.

### Fabrication of CHF and NTP-CHF

The wet-spinning technology was used for the fabrication of both a MWCNT hollow-fiber electrode (CHF) and NTP-incorporated CHF (NTP-CHF)[24,42]. Briefly, 4 g of MWCNTs (for CHF) or 3 g of MWCNTs with 1 g of NTP nanoparticles (for NTP-CHF) were dispersed in 34 g of N-methyl-2-pyrrolidone (NMP) by an ultrasonic homogenizer, and then 2 g of polyvinyl butyral (PVB) was added into the suspension as a dispersion stabilizer and binder. After five days of mixing, the homogeneous mixture was extruded through a hollow-fiber spinning apparatus with deionized water as a bore fluid. After the wet-spinning, hollow-fiber electrodes were dried at room temperature overnight, and then calcined at 350 °C for one hour in an Ar environment to remove PVB from the hollow-fiber electrode. It is worthy to note that >1 g of NTP nanoparticles in the spinning mixture induced a significant decrease in the mechanical strength during the preparation of NTP-CHF.

### Physicochemical characterization of CHF and NTP-CHF

The microstructure and morphology of CHF and NTP-CHF were observed using a scanning electron microscope (SEM; Magellan400, FEI) equipped with an energy dispersive X-ray spectrometer (EDS). An X-ray diffractometer (XRD; Rigaku SmartLab) was used to verify the presence of NTP nanoparticles in the NTP-CHF structure. The specific surface area and pore size distribution of CHF and NTP-CHF were evaluated by a Brunauer-Emmett-Teller analysis (BET; Tristar II 3020, Micrometrics). The electrochemical characteristics of the fabricated CHF and NTP-CHF electrodes were examined by a 3-electrode cell connected to an electrochemical working station (ZIVE SP1, WonA tech, Rep. of Korea) at the room temperature. CHF or NTP-CHF was used as working electrodes with a graphite rod as a counter electrode, and a saturated calomel electrode (SCE) as a reference electrode. A cyclic voltammetry (CV) analysis was carried out to determine electrochemical characteristics of CHF and NTP-CHF in 1.0 M (58,400 mg $L^{-1}$), 8.6 mM (500 mg $L^{-1}$), and 1.7 mM (100 mg $L^{-1}$) NaCl solutions as electrolytes with a 5 mV $s^{-1}$ scan rate. Here, 1.0 M NaCl solution was selected as a standard condition to evaluate the specific capacitance of the electrode, and 8.6 mM (500 mg $L^{-1}$) and 1.7 mM (100 mg $L^{-1}$) NaCl solutions were tested as feed solutions for the CDI process to meet the drinking water standard. The selective adsorption of $Na^+$ by NTP-CHF was measured in 1.0 M NaCl, 1.0 M $CaCl_2$, and 1.0 M NaCl with 50 mM $CaCl_2$ solutions with a 5 mV $s^{-1}$ scan rate. Unless otherwise specified, all electrode potentials are subsequently referred to as SCE.

### Ion capture and release test

The ion adsorption performance of CHF and NTP-CHF was evaluated in a batch-mode CDI cell at constant applied voltage of 1.3 V. In this cell, total 140 mg of CHF was used as an anode (positively polarized electrode), where 20 mg of CHF or NTP-CHF was used as the cathode (negatively polarized electrode) after the consideration of capacitance with 5 mm of the mean distance between anode and cathode (Supplementary Fig. 1). To evaluate the selective adsorption of $Na^+$ ions by NTP nanoparticles, $Ca^{2+}$ were chosen as representative cations due to their strong binding energy and abundance in natural waters[22,23,27]. The molar ratio of $Na^+$:$Ca^{2+}$ was varied from 100:0 to 100:5 by dissolving various amount of $CaCl_2$ at the fixed concentration of $Na^+$ (500 mg $L^{-1}$ or 8.6 mM of NaCl).

The concentration of $Na^+$ was measured by ion chromatography with cation column (Dionex Aquion IC, Thermo Fischer, USA), and $Ca^{2+}$ concentration was measured by a colorimetric method (HA-71A, Hach). The adsorption capacities of $Na^+$ and $Ca^{2+}$ were calculated by following equation:

$$\text{Cation adsorption capacity}\left(\text{mmol}\,g^{-1}\right) = \frac{(C_0 - C_f)\times V}{m_{cathode}} \quad (1)$$

where $C_0$ and $C_f$ are the initial and final concentrations (mM) of $Na^+$ or $Ca^{2+}$, respectively, $V$ is the volume of the solution in CDI cell (L), and $m_{cathode}$ is the mass of cathode electrodes (g).

## DATA AVAILABILITY

All data generated or analysed during this study are included in this published article and its Supplementary Information files.

Received: 22 September 2021; Accepted: 23 February 2022;
Published online: 19 April 2022

## REFERENCES

1. Porada, S., Zhao, R., van der Wal, A., Presser, V. & Biesheuvel, P. M. Review on the science and technology of water desalination by capacitive deionization. *Prog. Mater. Sci.* **58**, 1388–1442 (2013).
2. Bales, C., Kovalsky, P., Fletcher, J. & Waite, T. D. Low cost desalination of brackish groundwaters by Capacitive Deionization (CDI) – Implications for irrigated agriculture. *Desalination* **453**, 37–53 (2019).
3. Yang, J., Zou, L., Song, H. & Hao, Z. Development of novel $MnO_2$/nanoporous carbon composite electrodes in capacitive deionization technology. *Desalination* **276**, 199–206 (2011).
4. Gu, X., Yang, Y., Hu, Y., Hu, M., Huang, J. & Wang, C. Facile fabrication of graphene–polypyrrole–Mn composites as high-performance electrodes for capacitive deionization. *J. Mater. Chem. A* **3**, 5866–5874 (2015).
5. Hou, C.-H., Huang, J.-F., Lin, H.-R. & Wang, B.-Y. Preparation of activated carbon sheet electrode assisted electrosorption process. *J. Taiwan Inst. Chem. Eng.* **43**, 473–479 (2012).
6. Kim, C., Srimuk, P., Lee, J., Fleschmann, S., Aslan, M. & Presser, V. Influence of pore structure and cell voltage of activated carbon cloth as a versatile electrode material for capacitive deionization. *Carbon* **122**, 329–335 (2017).
7. Wang, H., Yan, T., Shen, J., Zhang, J., Shi, L. & Zhang, D. Efficient removal of metal ions by capacitive deionization with straw waste derived graphitic porous carbon nanosheets. *Environ. Sci.: Nano* **7**, 317–326 (2020).
8. Hsu, C.-C., Tu, Y.-H., Yang, Y.-H., Wang, J.-A. & Hu, C.-C. Improved performance and long-term stability of activated carbon doped with nitrogen for capacitive deionization. *Desalination* **481**, 114362 (2020).
9. Khan, Z. U., Yan, T., Han, J., Shi, L. & Zhang, D. Capacitive deionization of saline water using graphene nanosphere decorated N-doped layered mesoporous carbon frameworks. *Environ. Sci.: Nano* **6**, 3442–3453 (2019).
10. Quan, X. et al. Capacitive deionization of NaCl solutions with ambient pressure dried carbon aerogel microsphere electrodes. *RSC Adv.* **7**, 35875–35882 (2017).
11. Luo, G., Wang, Y., Gao, L., Zhang, D. & Lin, T. Graphene bonded carbon nanofiber aerogels with high capacitive deionization capability. *Electrochim. Acta* **260**, 656–663 (2018).
12. Zhang, S., Wang, Y., Han, X., Cai, Y. & Xu, S. Optimizing the fabrication of carbon nanotube electrode for effective capacitive deionization via electrophoretic deposition strategy. *Prog. Nat. Sci.: Mater. Int.* **28**, 251–257 (2018).
13. Gao, T., Zhou, F., Ma, W. & Li, H. Metal-organic-framework derived carbon polyhedron and carbon nanotube hybrids as electrode for electrochemical supercapacitor and capacitive deionization. *Electrochim. Acta* **263**, 85–93 (2018).
14. Li, J., Ji, B., Zhang, P., Chen, N., Zhang, G. & Qu, L. Hierarchical hole-enhanced 3D graphene assembly for highly efficient capacitive deionization. *Carbon* **129**, 95–103 (2018).
15. Divyapriya, G., Vijayakumar, K. K. & Nambi, I. Development of a novel graphene/$Co_3O_4$ composite for hybrid capacitive deionization system. *Desalination* **451**, 102–110 (2019).
16. Wu, T., Wang, G., Wang, S., Zhan, F., Fu, Y., Qiao, H. & Qiu, J. Highly stable hybrid capacitive deionization with a $MnO_2$ anode and a positively charged cathode. *Environ. Sci. Technol. Lett.* **5**, 98–102 (2018).
17. Li, H., Leong, Z. Y., Shi, W., Zhang, J., Chen, T. & Yang, H. Y. Hydrothermally synthesized graphene and $Fe_3O_4$ nanocomposites for high performance capacitive deionization. *RSC Adv.* **6**, 11967–11972 (2016).
18. Wang, Z., Xu, X., Kim, J., Malgras, V., Mo, R., Li, C., Lin, Y., Tan, H., Tang, J., Pan, L., Bando, Y., Yang, T. & Yamauchi, Y. Nanoarchitectured metal–organic framework/polypyrrole hybrids for brackish water desalination using capacitive deionization. *Mater. Horiz.* **6**, 1433–1437 (2019).
19. Szymczyk, A., Labbez, C., Fievet, P., Vidonne, A., Foissy, A. & Pagetti, J. Contribution of convection, diffusion and migration to electrolyte transport through nanofiltration membranes. *Adv. Colloid Interface Sci.* **103**, 77–94 (2003).
20. Yang, K.-L., Ying, T.-Y., Yiacoumi, S., Tsouris, C. & Vittoratos, E. S. Electrosorption of Ions from Aqueous Solutions by Carbon Aerogel: An Electrical Double-Layer Model. *Langmuir* **17**, 1961–1969 (2001).
21. Avraham, E., Noked, M., Cohen, I., Soffer, A. & Aurbach, D. The dependence of the desalination performance in capacitive deionization processes on the electrodes PZC. *J. Electrochemical Society* **158**,168–173 (2011).
22. Lado, J. J., Pérez-Roa, R. E., Wouters, J. J., Isabel Tejedor-Tejedor, M. & Anderson, M. A. Evaluation of operational parameters for a capacitive deionization reactor employing asymmetric electrodes. *Sep. Purif. Technol.* **133**, 236–245 (2014).
23. Mossad, M. & Zou, L. A study of the capacitive deionisation performance under various operational conditions. *J. Hazard Mater.* **213-214**, 491–497 (2012).

24. Lee, M.-Y., Kim, H., Kim, J.-O. & Kang, S. Three-dimensional hollow fiber type of carbon nanotube electrode for enhanced ion adsorption capacity. *Desalination Water Treat.* **90**, 46–53 (2017).
25. Zhi, M., Xiang, C., Li, J., Li, M. & Wu, N. Nanostructured carbon-metal oxide composite electrodes for supercapacitors: a review. *Nanoscale* **5**, 72–88 (2013).
26. Kim, D.-H., Choi, Y.-E., Park, J.-S. & Kang, M.-S. Capacitive deionization employing pore-filled cation-exchange membranes for energy-efficient removal of multi-valent cations. *Electrochim. Acta* **295**, 164–172 (2019).
27. Iglesias, G. R., Ahualli, S., Fernández, M. M., Jiménez, M. L. & Delgado, A. V. Soft electrodes in water desalination: application to multi-valent ions. *Environ. Sci.: Water Res. Technol.* **5**, 873–883 (2019).
28. Wu, C., Kopold, P., Ding, Y.-L., van Aken, P. A., Maier, J. & Yu, Y. Synthesizing Porous $NaTi_2(PO_4)_3$ nanoparticles embedded in 3D Graphene Networks for high-rate and long cycle-life sodium electrodes. *ACS Nano* **9**, 6610-6618 (2015).
29. Guo, Z., Ma, Y., Dong, X., Hou, M., Wang, Y. & Xia, Y. Integrating desalination and energy storage using a saltwater-based hybrid sodium-ion supercapacitor. *ChemSusChem* **11**, 1741–1745 (2018).
30. Wang, K., Liu, Y., Ding, Z., Li, Y., Lu, T. & Pan, L. Metal–organic-frameworks-derived NaTi2(PO4)3/carbon composites for efficient hybrid capacitive deionization. *J. Mater. Chem. A* **7**, 12126–12133 (2019).
31. Shanbhag, S., Bootwala, Y., Whitacre, J. F., & Mauter, M. S. Ion transport and competition effects on NaTi2(PO4)3 and Na4Mn9O18 selective insertion electrode performance. *Langmuir* **33**, 12580–12591 (2017).
32. Cretin, M. & Fabry, P. Detection and selectivity properties of $Li^+$-ion-selective electrodes based on NASICON-type ceramics. *Analytica Chim. Acta* **354**, 291–299 (1997).
33. Wu, X.-Y., Sun, M.-Y., Shen, Y.-F., Qian, J.-F., Cao, Y.-L., Ai, X.-P. & Yang, H.-X. Energetic aqueous rechargeable sodium-ion battery based on $Na_2CuFe(CN)_6$ -$NaTi_2(PO_4)_3$ intercalation chemistry. *ChemSusChem* **7**, 407–411 (2014).
34. Choi, W., Shin, H.-C., Kim, J. M., Choi, J.-Y. & Yoon, W.-S. Modeling and Applications of Electrochemical Impedance Spectroscopy (EIS) for Lithium-ion Batteries. *J. Electrochem. Sci. Technol.* **11**, 1–13 (2020).
35. Eftekhari, A. The mechanism of ultrafast supercapacitors. *J. Mater. Chem. A* **6**, 2866–2876 (2018).
36. Kim, T. & Yoon, J. CDI ragone plot as a functional tool to evaluate desalination performance in capacitive deionization. *RSC Adv.* **5**, 1456–1461 (2015).
37. Lee, J.-H., Bae, W.-S. & Choi, J.-H. Electrode reactions and adsorption/desorption performance related to the applied potential in a capacitive deionization process. *Desalination* **258**, 159–163 (2010).
38. Chen, F., Huang, Y., Kong, D., Ding, M., Huang, S. & Yang, H. $NaTi_2(PO_4)_3$-Ag electrodes based desalination battery and energy recovery. *FlatChem* **8**, 9–16 (2018).
39. Hou, C.-H. & Huang, C.-Y. A comparative study of electrosorption selectivity of ions by activated carbon electrodes in capacitive deionization. *Desalination* **314**, 124–129 (2013).
40. Noda, Y., Nakano, K., Otake, M., Kobayashi, R., Kotobuki, M., Lu, L., & Nakayama, M. Research Update: Ca doping effect on the Li-ion conductivity in NASICON-type solid electrolyte $LiZr_2(PO_4)_3$: A first-principles molecular dynamics study. *APL Materials* **6**, 060702 (2018).
41. Tamura, S., Yamane, M., Hoshino, Y. & Imanaka, N. Highly conducting divalent $Mg^{2+}$ cation solid electrolytes with well-ordered three-dimensional network structure. *J. Solid State Chem.* **235**, 7–11 (2016).
42. Fan, X., Liu, Y., Quan, X., Zhao, H., Chen, S., Yi, G. & Du, L. High desalination permeability, wetting and fouling resistance on superhydrophobic carbon nanotube hollow fiber membrane under self-powered electrochemical assistance. *J. Membr. Sci.* **514**, 501–509 (2016).

## AUTHOR CONTRIBUTIONS

J.P. - Conceptualization, Software, Writing original draft; M.Y.L. - Methodology, Investigation, Data curation; S.H. - Material preparation, Measurement; K.L. - Investigation, Resources; S.K. - Supervision, Reviewing and Editing, Project administration, Funding acquisition.

## FUNDING

This work was supported by the National Research Foundation of Korea (NRF) grant funded by the Korea government (MSIT) (NRF-2020R1A2C3012639).

## COMPETING INTERESTS

The authors declare no competing interests.

## ADDITIONAL INFORMATION

**Supplementary information** The online version contains supplementary material available at https://doi.org/10.1038/s41545-022-00156-3.

**Correspondence** and requests for materials should be addressed to Seoktae Kang.

**Reprints and permission information** is available at http://www.nature.com/reprints

**Publisher's note** Springer Nature remains neutral with regard to jurisdictional claims in published maps and institutional affiliations.